

# MULTIPLE PRODUCTION, TRANSPORT IN ATMOSPHERE AND DETECTION OF HIGH ENERGY COSMIC RAYS

JEAN-NOËL CAPDEVIELLE, FABRICE COHEN AND CORENTIN LE GALL  
*PCC, Collège de France, 11, Place Marcelin Berthelot, 75231 Paris Cédex 05 France*  
*E-mail: capdev@cdf.in2p3.fr*

IZABELA KURP, BARBARA SZABELSKA AND JACEK SZABELSKI  
*The Andrzej Soltan Institute for Nuclear Studies, 90-950 Łódź 1, Box 447, Poland*  
*E-mail: js@zpk.u.lodz.pl*

We describe the general aspects of Monte Carlo Collision Generators suitable for cosmic ray nucleon-Air and nuclei-Air interactions, including accelerator and collider data. The problem of the extrapolation at 3 energy decades above the LHC of the main features of high energy collisions is discussed and under theoretical and phenomenological assumptions, the properties of the longitudinal and lateral development of giant extensive air showers simulated with the CORSIKA program are presented. The determination of the primary energy near  $10^{20}$  eV is examined for different observables, total size, densities of charged particles interpolated at 600 m from shower core.

The extensive air shower data collected around LHC energy is in better agreement with models of large multiplicities. Beyond this energy, the extrapolation carried assuming the diquark breaking mechanism can change the classic conversion to primary energy and such circumstance can have consequences on the validity of the GZK cut off.

In those conditions, we have simulated large and giant air showers taking into account, in addition, new processes, such as diquark breaking, and topological problems involving adequate structure functions for lateral distributions, up to energies exceeding  $10^{20}$  eV for P.AUGER and EUSO experiments.

## 1 Monte Carlo Collision generators for Cosmic Rays and extrapolation at ultra high energy

In order to simulate in a reasonable time the 4-dimensional development of Extensive Air Showers at very high energy, it is important to elaborate collision generators reproducing rapidly the detailed features of multiple production observed in accelerators and colliders. Among the variety of models implemented in CORSIKA, there are microscopic and phenomenological models. The first ones include all the steps of the parton momenta generation from the parton distribution functions related to valence quarks and diquarks, sea quarks and gluons, convoluted with the fragmentation of the respective strings into secondary hadrons. The phenomenological models provide fast and direct hadron sampling, but take into account some global characteristics of the

Gribov-Regge theories with parameters adjusted to the experimental data. One common feature is the separation between the non single diffractive component and the diffractive component (single and double) with the inclusion of soft and hard mechanisms.

As an example (fig.1), the reproduction of the inclusive data with the model HDPM2 (2nd version of the hybrid dual parton model) with parameters tuned to fit the experimental data of FermiLab at  $\sqrt{s} = 630 GeV$  gives a total average inelasticity for p-p collisions of 0.7 instead of 0.5 when adjusted to the previous measurements of UA5. The forward trajectory on Fig. 1 is not constrained above 5.5 units of pseudo rapidity and several models taken in option for CORSIKA can have different trajectories in the forward region with a good agreement to the observed data, but rather different inelasticities. A cosmic ray cascade is initiated by the unique interaction of the primary particle and the fluctuations of the elementary act have to be reproduced carefully taking into account the semi-inclusive data as well as the correlation between charged and neutral secondaries. The extrapolation at ultra high energy can be carried with the model HDPM2 taking into account recent features of collider physics such as  $p_t$  versus central rapidity density (UA1-MIMI exp.) and recent results of FermiLab <sup>1</sup> for pseudo-rapidity up to 5.5. The pseudo-rapidity distributions obtained <sup>2</sup> with HDPM2 for 2000 collisions NSD are shown on Fig. 1. The distributions on Fig. 1 (histograms for HDPM2, full line for QS-JET model) give for HDPM2 different extrapolations at  $10^{10}$  GeV following the PDF assumed ( $B_0$  and  $B_-$ ).

The correlation between the central rapidity density and the average transverse momentum  $\langle p_t \rangle$  plays also one role in the muon and hadron radial distributions: the dependence of the transverse momentum on energy turns to a permanent increase on Fig. 1.

The p-p collision is transformed to p-A collision following Glauber's considerations and Nuclei-Air collisions are treated by the abrasion evaporation procedure.

## 2 Simulation of giant EAS

The electromagnetic cascade is treated by EGS4 involving cross sections, taking into account the LPM effect, for bremsstrahlung and pair production. The nuclear photo production has been implemented in the simulation and its contribution is compared versus the primary photon energy to the previous processes on the Fig. 2 <sup>2</sup>.

The fluctuations of multiplicity are governed by the negative binomial distribution and at  $10^{20} eV$ , the average charged multiplicity is close to

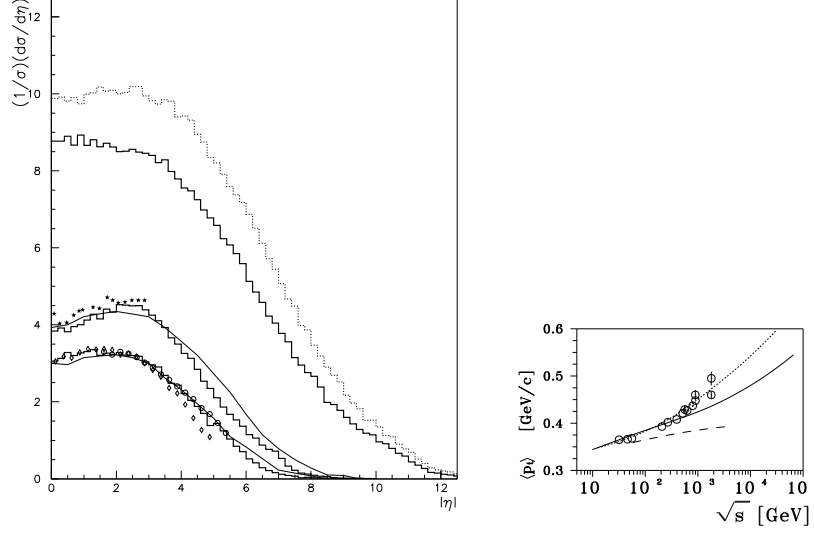


Figure 1. Left: pseudo-rapidity distribution with HDPM2. Right: average  $p_t$  vs. energy dependence with HDPM2.

300 for HDPM (1000 for QGSJET); this corresponds to energy densities of  $30 \text{ GeV}/fm^3$  in average... and we have not considered here the important modifications from a possible phase transition to QGP.

The longitudinal developments obtained for proton, photon and iron induced extensive air showers are compared on Fig. 2. We notice that the showers (here averaged on 10 individual cascades simulated with CORSIKA) have their maximum near 1000–1500 m altitude for proton and iron. The  $\gamma$  shower initiated at  $50 \text{ g}/cm^2$  exhibits a different behaviour due to the LPM effect; a rule of thumb for hadronic showers is to divide by 2 the total energy in  $\text{GeV}$  to get  $N_{max}$ . This maximum depth corresponds to a minimum of fluctuations, suggested by analytic cascade theory and confirmed by the Monte Carlo simulation, indicating the well adapted localisation of AGASA and AUGER experiments. The depth of the maximum depends on the logarithm of the primary energy, when  $N_{max}$  remains proportional to energy with a similar factor for a large variety of interaction models.

A more delicate problem is the estimation of  $N_{max}$ ; it can be read directly from the cascade curve derived from fluorescence measurements, as performed

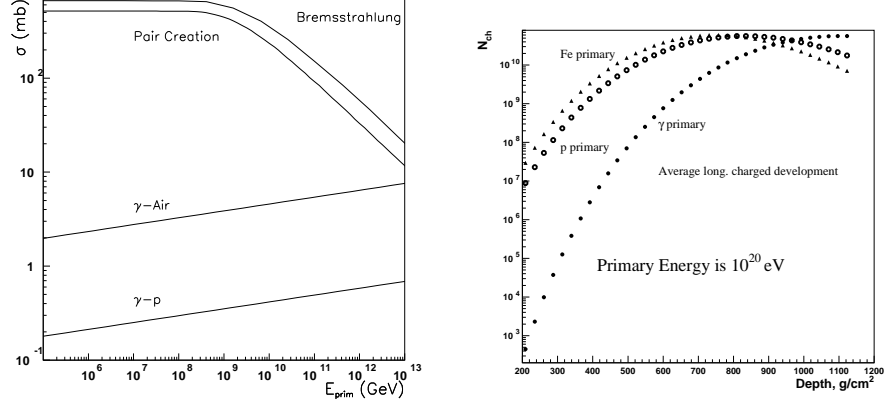


Figure 2. Left: Photo-production cross section in air compared with bremsstrahlung and pair production cross sections reduced by the LPM effect. Right: longitudinal development of EAS for  $\gamma$ , p and Fe primaries.

by the Fly's Eye or Hires, but the approach with a small number of detectors hit at large distances (1 to 1.5 km) turns to a hopeless topological problem.

### 3 Topological aspects of radial distribution

The profile of the lateral distribution assumed and the method of core localization are especially important. We propose instead of NKG and other Euler Beta functions, the employment of the gaussian hypergeometric formalism giving also normalization and better skewness, under the form:

$$f(x) = g(s)x^{s-a}(x+1)^{s-b}(1+dx)^{-c} \quad (1)$$

which has the advantage (for values of parameters respecting the conditions of convergence  $s-a+2 > 0$  and  $c-2s+b-2 > 0$ ) to be exactly normalized in terms of Gaussian Hypergeometric function  $F_{HG} = F(c, s-a+2, c+b-s; 1-d)$  by:

$$g(s) = \frac{\Gamma(c+b-s)}{2\pi\Gamma(s-a+2)\Gamma(c-2s+b+a-2)F_{HG}} \quad (2)$$

The empirical distributions, such as AGASA function <sup>3</sup>, as underlined by Vishwanath <sup>4</sup> enters in the category of Hypergeometric Gaussian functions <sup>5</sup>,

Table 1. Best parameters to simulated  $e^+e^-$  + muons (all charged) lateral distribution fit using JNC01 formula.

	p10	p20	Fe10	Fe20
$\log_{10}N_e$	10.75	10.72	10.70	10.65
$r_M$	21.26	21.26	19.18	19.18
$r_0$	8785.	8785.	9536.	9536.
$a$	1.91	1.91	1.82	1.82
$s$	1.03	1.04	1.03	1.04
$b$	3.32	3.32	3.31	3.31
$\beta$	10.0	10.0	10.0	10.0

under the general form of structure function

$$f(x) = C_e \cdot x^{-\alpha} \cdot (1+x)^{-(\eta-\alpha)} \cdot (1+dx)^{-\beta} \quad (3)$$

with the conditions  $2-\alpha > 0$  and  $\beta + \eta - 2 > 0$ . The value used in AGASA function for the coefficient  $C_e$  is just an approximation; the exact value is

$$C_e = \frac{\Gamma(\beta + \eta - \alpha)}{2\pi \cdot \Gamma(2 - \alpha) \cdot \Gamma(\beta + \eta - 2)} \cdot \frac{1}{F_{HG}}$$

where  $F_{HG} = F_{HG}(\beta, 2 - \alpha, \beta + \eta - \alpha; 1 - d)$ . The Hypergeometric Gaussian function can be easily calculated from the hypergeometric series:

$$F_{HG}(a, b, c; z) = \sum_{n=0}^{\infty} \frac{(a)_n (b)_n}{(c)_n n!} z^n, \quad c \neq 0, -1, -2, \dots,$$

$$(a)_n = \Gamma(a + n) / \Gamma(a), \quad (a)_0 = 1$$

This equation is equivalent to our version (3) containing the age parameter  $s$  with the relations between respective coefficients:  $x = \frac{r}{r_M}$ ,  $d = \frac{r_M}{r_0}$ ,  $s = 1.03$ ,  $\alpha = a - s$ ,  $\eta = b - s + \alpha$  (the value of  $s$  is taken from the longitudinal development simulated).

We have adjusted with MINUIT the parameters of our hypergeometric function (Table 1) to the average lateral distributions (set JNC01 for charged, JNC02 for electrons) of groups of 10 showers at  $10^{20}$  eV simulated with CORSIKA (QGSJET model), as shown on Fig. 3.

In each case, the adjustment has been performed with 50 points from the simulation distributed from 0.1 m up to 10 km from axis position for charged particles (muons and electrons). The advantages of JNC01 formula can be seen on Fig. 3 and on Table 2.

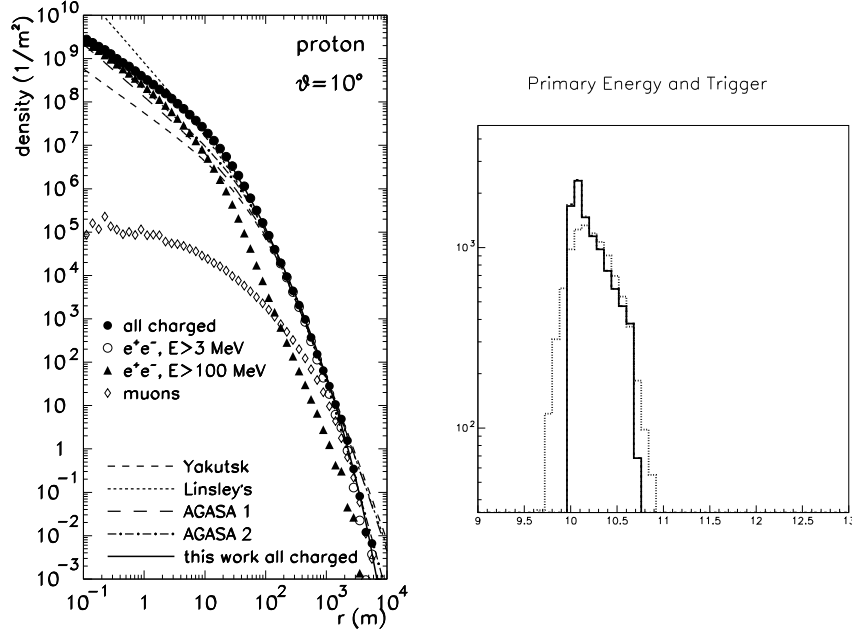


Figure 3. Left: fits to all charged particles lateral distribution from simulations (average from 10 EAS). Primary particle is a proton with energy  $10^{11}$  GeV. Lines are normalized to  $\varrho(600 \text{ m})$ . Right: extra component to GZK's cut off in case of diquark breaking. Full line: generated spectrum, dashed: reconstructed, versus  $\log_{10}(E_0/1 \text{ GeV})$

The major part of the particles is contained inside 200 m from the axis and only the skewness of the hypergeometric function allows a reliable relation between size and density at 600 m. This function has been applied to localizations of the showers contained in the catalogues of Volcano Ranch and Yakutsk. The core position has been obtained by minimization with Minuit program between different formulas available for lateral densities written versus the coordinates  $X, Y$  as

$$\varrho(r) = \varrho(\sqrt{(X - X_c)^2 + (Y - Y_c)^2}) \quad (4)$$

where the core coordinates  $X_c$  and  $Y_c$  are taken as two additive parameters in the minimization. The adjustments are generally improved when compared to the original treatments, turning to lower sizes (in the case of Yakutsk formula)

Table 2. Columns *a* present total number of charged particles  $N_e$  in  $10^{10}$ , columns *b* the ratios  $E_0/N_e$  in GeV ( $E_0=10^{11}$  GeV) and columns *c* the ratios  $\varrho(600)/N_e$  in  $10^{-8}$  particles/m<sup>2</sup>.  $m(600) = \frac{d(\log \varrho)}{d(\log r)}$  at 600 m.

	proton 10°			proton 20°			iron 10°			iron 20°		
$\varrho(600)$	290 m <sup>-2</sup>			318 m <sup>-2</sup>			369 m <sup>-2</sup>			356 m <sup>-2</sup>		
$E_0/\varrho(600)$ (GeV m <sup>2</sup> )	$3.4 \cdot 10^8$			$3.1 \cdot 10^8$			$2.7 \cdot 10^8$			$2.8 \cdot 10^8$		
$m(600)$	-3.9			-3.6			-3.6			-4.0		
fit	1a	1b	1c	2a	2b	2c	3a	3b	3c	4a	4b	4c
Yakutsk	1.8	5.6	1.6	1.7	5.9	1.9	2.3	4.3	1.6	1.9	5.3	1.8
Linsley's	8.2	1.2	0.3	8.0	1.3	0.3	10.5	0.9	0.3	8.9	1.1	0.4
AGASA#1	2.4	4.2	1.2	2.6	3.8	1.2	3.1	3.2	1.1	2.9	3.4	1.2
AGASA#2	3.3	3.0	0.8	3.6	2.8	0.8	4.2	2.4	0.8	4.0	2.5	0.8
this work	5.6	1.8	0.5	5.6	1.9	0.6	5.1	2.0	0.7	4.5	2.2	0.7

Table 3. Localization of the most energetic AGASA event:  $\chi^2$ ,  $\varrho(600)$ ,  $N_e$  and relative core distance from the original localization. Age parameter *s* fitted for A and B functions as 1.05 and 0.98, respectively.

	$\chi^2/23$	$\varrho(600)$ (1/m <sup>2</sup> )	$N_e$ ( $10^{10}$ )	$\Delta r$ (m)
original		892	7.84	0.00
A – JNC01	7.32	598	34.81	82.44
B – JNC02	8.24	599	17.57	98.83
C – Yakutsk	10.40	561	3.01	101.15
D – Linsley's	7.51	565	10.74	83.29
E – AGASA no. 1	6.90	580	6.43	77.10
F – AGASA no. 2	11.81	611	8.92	60.49

and better approximation of the density at 600 m. The situation of the most energetic event of AGASA <sup>6</sup> is given in Table 3.

#### 4 Fluorescence, Cerenkov and Radio emissions

From the longitudinal development, we have developed a method of fast simulation based on the structural stability of the subshowers (in the sense of catastrophe theory). This is an efficient alternative to the thinning technique. The lateral extension of the total amount of light received at a fixed distance from the axis is compared for both Cerenkov and fluorescence component and

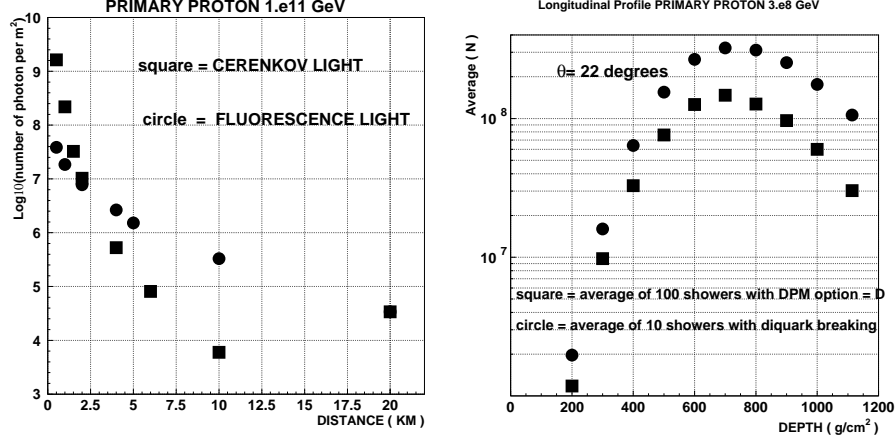


Figure 4. 1. Cerenkov and fluorescence light for a proton at  $10^{20}$  eV. - 2. Simulation with DPM model with option D (100 showers), and diquark breaking (10 showers).

shown on Fig. 4.

The opportunity of CORSIKA which separates positive and negative particles taught us that a regular negative excess close to 25% is present in the e.m. component of EAS, allowing the calculation of radio emission, following Askarian's effect. In Yakutsk experiment, it is possible to estimate the primary energy from the density at 600 m as well as from the Cerenkov component; in AUGER array, the direct calibration of showers detected simultaneously by the ground array and the fluorescence detector looks promising.

## 5 Diquark breaking mechanism and GZK cut off

The diquark breaking mechanism disturbs strongly the leading particle effect present in the different models used in cosmic rays. In the classical form of the dual parton model, the 3 valence quarks of the proton projectile are separated in a fast diquark and another valence quark slowed down. The diquark is recombined with one quark of the sea to produce, the most commonly, an outgoing leader baryon propagating the energy deeper in the cascade. The 3 valence quarks separated will be recombined in various meson structures in pairs  $|u\bar{d}\rangle$ ,  $|d\bar{u}\rangle$ , ... or neutral mesons as  $1/\sqrt{2}(d\bar{d} - u\bar{u})$ . The configuration with the simultaneous final state for the valence quarks of  $3\pi^0$ 's could



be especially interesting with a probability of emergence that we can evaluate from the quark content and the quark additive model as  $1/27$ . Such configuration (with intermediate final states of higher probabilities, one pair of charged pions and one neutral, one pair of neutral and one charged...) will transfer a large part of energy to the electromagnetic component and this energy will be definitely missing for both hadronic and penetrating components. Remembering that for the same primary energy, the cascade theory shows that one primary photon produces at maximum, approximately, two times more electrons, we can expect a large electron excess for some cascades initiated with diquark breaking. The longitudinal development calculated for protons of the same energy of  $3 \cdot 10^8$  GeV is compared to a classical development, here the model HDPM2 with D-option, on Fig. 4. The electron size at maximum is doubled in the assumption of diquark breaking and relatively rare recombination simultaneously in 3 neutral pions<sup>11</sup>. We have simulated  $10^4$  showers, between 10 *EeV* and 50 *EeV*, where the generation, following the primary energy differential spectrum, is cut by brute force. The showers simulated with axis distributed randomly are treated following the method of AGASA and the primary spectrum reconstructed is superimposed on the original one. It appears an extra component above 50 *EeV*, due to the showers including the diquark mechanism, considered previously, and such artefact could appear as a GZK violation. With AUGER array, such showers could be recognized very easily by an energy 3 or 4 times larger from the fluorescence detector than estimated by the water tank detectors. We observed also that such artificial component could appear from spacial topological situations at 50 *EeV*; for instance, with an axis falling near one detector, all the others are hit by densities near the low density threshold and the answer very unstable of those surrounding detectors can turn to an important overestimation of the primary energy.

## 6 Conclusions

The hypergeometric approach gives a better accuracy in the interpolation of densities at 600–1000 m, a more reliable estimation of the shower size (when the axis is in the array), a better axis localization and finally a more correct constraint of the primary energy. The position of the axis is crucial as the density near 600 m varies as  $r^{-4}$  and an uncertainty of 50 m on axis turns to an error of 40% at least on primary energy. Topological difficulties and also non standard aspect of multiple production needs probably more attention to be able to rule out definitely the cut off of GZK.

## Acknowledgments

This work has been partly supported (JNC, FC and CLG) by INTAS contract 1339.

## References

1. Capdevielle J.N. et al. in Proc. 26<sup>th</sup> ICRC (Salt Lake City) 1 1999 111.
2. Capdevielle J. N., Le Gall C., Sanosyan K. in Astroparticle Physics 13 2000 259.
3. Nagano M. et al. in J. Phys. G.: Nucl. Particle Phys. 18 1992 423.
4. Vishwanath P. R. in Proc. 23<sup>rd</sup> ICRC (Calgary), Rapporteur Papers 6 1993 384.
5. Capdevielle J. N., Procureur J. in Proc. 18th ICRC 11 1983 307.
6. Yoshida S. et al. in Astroparticle Physics 3 1995 105.
7. Saltzberg, D. et al., preprint hep-ex/0011001, 2000.
8. Askaryan, G. A., Zh. Exp. Theor. Phys., 41 616 1961.
9. Capdevielle J.N. et al. in J. Phys. G 14 1988 503.
10. Capdevielle J.N. et al. in Proc. 24<sup>th</sup> ICRC (Roma) 1 1995 910.
11. Nikolsky, S. I., Romakhin, V. A., Physics of Atomic Nuclei, 63 10 1799 2000.
12. Attallah R., Capdevielle J.N., Meynadier C. and Szabelski J. in J. Phys. G 22 1997 1497;